Water Research 202 (2021) 117408

Contents lists available at ScienceDirect

Water Research

journal homepage: www.elsevier.com/locate/watres

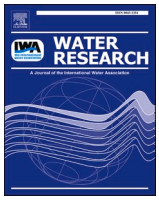

Degradation and deactivation of plasmid-encoded antibiotic resistance genes during exposure to ozone and chlorine

Younggun Yoon [a,1], Huan He [b,1], Michael C. Dodd [b,*], Yunho Lee [a,*]

[a] School of Earth Sciences and Environmental Engineering, Gwangju Institute of Science and Technology (GIST), Gwangju 61005, Republic of Korea
[b] Department of Civil and Environmental Engineering, University of Washington, Seattle, WA 98195, United States

ARTICLE INFO

Keywords:
Antibiotic resistance genes
Gene transformation
Ozone
Chlorine
Radicals
DNA repair

ABSTRACT

Degradation and deactivation kinetics of an antibiotic resistance gene (ARG) by ozone (O_3) and free available chlorine (FAC) were investigated in phosphate-buffered solutions at pH 7 for O_3 (in the presence of *tert*-butanol), and pH 6.8 or 8.1 for FAC. We used a plasmid (pUC19)-encoded ampicillin resistance gene (amp^R) in both extracellular (e-) and intracellular (i-) forms. The second-order rate constant (k_{O3}) for degradation of 2686 base pair (bp) long e-pUC19 toward O_3, which was determined by quantitative polymerase chain reaction assay, was calculated to be $\sim 2 \times 10^5$ $M^{-1}s^{-1}$. The deactivation rate constants of e-pUC19 by O_3 measured with various recipient *E. coli* strains were within a factor of 2 compared with the degradation rate constant for e-pUC19. The degradation/deactivation kinetics of i-pUC19 were similar to those of e-pUC19, indicating only a minor influence of cellular components on O_3 reactivity toward i-pUC19. For FAC, the degradation and deactivation rates of e-pUC19 were decreased in the presence of *tert*-butanol, implying involvement of direct FAC as well as some radical (e.g., $^{\bullet}OH$) reactions. The degradation rates of e-amp^R segments by direct FAC reaction could be explained by a previously-reported two-step sequential reaction model, in which the rate constants increased linearly with e-amp^R segment length. The deactivation rate constants of e-pUC19 during exposure to FAC were variable by a factor of up to 4.3 for the different recipient strains, revealing the role of DNA repair in the observed deactivation efficiencies. The degradation/deactivation of e-pUC19 were significantly faster at pH 6.8 than at pH 8.1 owing to pH-dependent FAC speciation variation, whereas i-pUC19 kinetics exhibited much smaller dependence on pH, demonstrating intracellular plasmid DNA reactions with FAC occurred at cytoplasmic pH (~7.5). Our results are useful for predicting and/or measuring the degradation/deactivation efficiency of plasmid-encoded ARGs by water treatment with ozonation and chlorination.

1. Introduction

Increasing antibiotic resistance is a global threat to human and animal health as it has lowered the effectiveness of antibiotic treatment against bacterial infections (United Nations, 2019). Although antibiotic resistance occurs naturally, the overuse and misuse of antibiotics have accelerated its dissemination amongst bacterial communities by selecting bacteria carrying antibiotic resistance genes (ARGs) responsible for antibiotic resistance traits (Davies and Davies 2010).

ARGs are now considered as contaminants of concern in various aquatic environments, as ARG transfer via natural/anthropogenic water cycles can potentially contribute to the spread of antibiotic resistance to pathogens (Czekalski et al., 2012; Dodd 2012; Pruden et al., 2006). ARGs exist in aquatic environments within bacterial cells (i.e., intracellularly) but also extracellularly; where the latter are generated by lysis of dead cells or secretion from live cells (Zhang et al., 2018). Both extra- (e-) and intracellular (i-) ARGs are of concern considering the potential for dissemination of antibiotic resistance (Dodd 2012; Nagler et al., 2018). Antibiotic resistance can be disseminated within bacterial populations by sharing of mobile ARGs contained within bacteriophages, plasmids, and chromosomal DNA through horizontal gene transfer (HGT) processes including conjugation (cell-to-cell contact), transduction (viral delivery), and transformation (uptake of free DNA) (Thomas and Nielsen 2005).

Disinfection and oxidation of drinking water and wastewater serve as important barriers to the spread of pathogenic microorganisms in urban

* Corresponding authors.
E-mail addresses: doddm@uw.edu (M.C. Dodd), yhlee42@gist.ac.kr (Y. Lee).
[1] Y. Yoon and H. He contributed equally to this work.

https://doi.org/10.1016/j.watres.2021.117408
Received 11 February 2021; Received in revised form 29 June 2021; Accepted 30 June 2021
Available online 6 July 2021

water systems (Jacangelo and Trussell 2002). Free available chlorine (FAC) and ozone (O_3) are widely used for disinfection, and O_3 is also employed for chemical contaminant elimination (von Gunten 2018; Von Sonntag and Von Gunten 2012). The efficacy of water disinfection and oxidation processes in mitigating ARGs has received increasing attention (Dodd 2012). Various studies have employed quantitative polymerase chain reaction (qPCR) assays of DNA damage to show that FAC and O_3 are capable of degrading ARGs (Alexander et al., 2016; Czekalski et al., 2016; He et al., 2019; Pak et al., 2016; Yoon et al., 2017; Zhang et al., 2019). However, fundamental kinetic parameters (e.g., bimolecular rate constants) and molecular-level reaction models for ARG degradation by these oxidants are still scarce, which has hindered comparison and generalization of ARG removal efficacies by different water disinfectants/oxidants. Only a limited number of recent studies have reported such information on the degradation of plasmid-borne and/or chromosomal ARGs (He et al., 2019; Nihemaiti et al., 2020; Yoon et al., 2018), and none of these have specifically addressed O_3 reactions with *plasmid-borne* ARGs. Furthermore, kinetics of ARGs' *deactivation* (i.e., loss of ARG transforming activity – where transforming activity is defined here as the ability of an intact ARG to confer a resistance trait to a non-resistant bacterial cell via the HGT process of transformation) have been investigated in only a few studies (Chang et al., 2017; He et al., 2019; Nihemaiti et al., 2020; Yoon et al., 2018), none of which have focused specifically on the deactivation of *plasmid-borne* ARGs by O_3 and FAC.

qPCR methods have been widely used to quantify structurally-intact ARGs and monitor their degradation in water disinfection/oxidation (Alexander et al., 2016; Chang et al., 2017; Czekalski et al., 2016; He et al., 2019; McKinney and Pruden 2012; Yoon et al., 2017; Yoon et al., 2018; Zhang et al., 2019). However, it is important to note that most qPCR methods monitor only a part of a target ARG's sequence (e.g., segment sizes of 200–1000 base pairs [bps]), but not the entire sequence related to the biological activity of the ARG. Thus, short segment-based (e.g., ~200 bps) qPCR methods may underestimate ARG damage and associated loss of ARG transforming activity (Chang et al., 2017; He et al., 2019; Yoon et al., 2018). Moreover, qPCR methods do not simulate uptake and repair of DNA by recipient bacterial cells, which can play important roles in modulating transforming activity of ARGs (Chang et al., 2017; Yoon et al., 2018). In addition, the DNA replication efficiency in qPCR methods can be different from that in bacterial cells subjected to gene transformation (e.g., due to differences in DNA polymerases). Correlations between the degradation of target ARG segments (typically measured by qPCR) and the removal of ARG transforming activity (measured by transformation assay) have been found for some plasmid-borne (Chang et al., 2017; Nihemaiti et al., 2020; Yoon et al., 2018) as well as chromosomal ARGs (He et al., 2019) during treatment with certain water disinfectants and oxidants, with explanations hypothesized based on molecular mechanisms of DNA transformation for the relevant bacterial strains (He et al., 2019; Nihemaiti et al., 2020; Yoon et al., 2018). Nevertheless, further study is needed of the relationships between degradation and deactivation of ARGs by O_3 and FAC.

This investigation was in turn undertaken with the goals of (i) providing carefully-determined kinetics parameters for degradation *and* deactivation of plasmid-borne ARGs by O_3 and FAC, (ii) improving the fundamental understanding of how O_3 and FAC contribute to damage of plasmid DNA and how that relates to observed ARG degradation and deactivation kinetics, and (iii) investigating the role of DNA damage repair in governing observed ARG deactivation kinetics by each oxidant. An overarching aim of this work was to advance the quantitative and conceptual foundations for characterizing, modeling, and predicting the fate of plasmid-borne ARGs during water and wastewater chlorination and ozonation. A plasmid (pUC19) carrying an ampicillin resistance gene (amp^R) was used as an extracellular ARG (e-ARG), and *Escherichia coli* strain DH5α transformed with pUC19 was used to represent an intracellular ARG (i-ARG). The e- and i-pUC19 were prepared in phosphate-buffered solutions and exposed to different levels of O_3 (with *tert*-butanol) and FAC (without and with *tert*-butanol). The treated samples were analyzed by qPCR (for quantifying amp^R degradation), ARG transformation assays (for quantifying amp^R deactivation), and agarose gel electrophoresis. The observed kinetic behaviors were used to derive kinetic models and corresponding rate constants, and then applied to predict degradation rate constants for the entire pUC19 plasmid by each disinfectant. The ARG transformation assays employed five *E. coli* strains with varying DNA damage repair abilities, in order to assess the influence of DNA repair on observed ARG deactivation kinetics. Finally, degradation and deactivation kinetics of amp^R were compared and discussed with respect to explaining and predicting the elimination efficiency of ARG transforming activities.

2. Materials and methods

2.1. Standards and reagents

Chemicals and solvents (all of analytical grade or higher) were purchased from various commercial suppliers and used as received without further purification. Other reagents, culture media, and oxidant stock solutions are described in the Supporting Information (SI)-Text-1.

2.2. Preparation of E. coli cultures and plasmid DNA

E. coli K12 strain DH5α (*recA*$^-$, *endA*$^-$) – where the parenthetic term indicates a deletion of the specified genes by genetic modification – was obtained from the American Type Culture Collection (ATCC). *E. coli* K12 mutants AB2480 (*uvr*A$^-$, *rec*A$^-$), AB1186 (*uvr*A$^-$), AB2463 (*rec*A$^-$), and AB1157 (wild-type) were provided by the Coli Genetic Stock Center (CGSC) at Yale University. Cultures of *E. coli* K12 AB strains and DH5α were grown to concentrations of ~10^9 colony-forming units (CFU)/mL according to methods described elsewhere (Nihemaiti et al., 2020; Yoon et al., 2017). Cells from the mid-exponential growth phase were used in this study. Plasmid pUC19 (2686 bps) is a commercially available *E. coli* vector encoding an ampicillin resistance gene (amp^R, 861 bps). Plasmids were extracted from *E. coli* using the AccuPrep Nano-Plus Plasmid Extraction Kit (Bioneer), as described previously (Yoon et al., 2017). Plasmid concentrations were quantified with a NanoDrop ND-2000 spectrophotometer (NanoDrop Products, Wilmington, DE, USA). The concentrations of extracted plasmid stocks were 0.5–1 mg/mL (~3×10^{11} copies/μL).

2.3. Ozonation and chlorination experiments

pUC19 or *E. coli* DH5α cells were prepared separately in phosphate-buffered (PB) solutions (2 mM) at ~1 mg/L (3×10^{14} copies/mL or 3.2 μM of nucleotides) for the plasmid or ~5×10^6 CFU/mL for *E. coli*. These samples were treated with O_3 (70 μM) or FAC (70 − 560 μM) in bench-scale experiments in which the oxidant concentrations were in molar excess of DNA. To study the fast kinetics of O_3 reactions, a continuous-flow, quenched-reaction system was used according to procedures described previously (He et al., 2019). All O_3 experiments were carried out in the presence of *tert*-butanol (10 mM) to scavenge hydroxyl radical ($^{\bullet}$OH) (Flyunt et al., 2003b). Moreover, 10 mM of *tert*-butanol on its own had negligible effect on the amp^R segment in a control test conducted in the absence of O_3. Chlorination was performed in a batch reactor, without and with *tert*-butanol (10 mM) to investigate the possible influence of radical reactions. Further details of the ozonation and chlorination experiments are provided in SI-Text-2.

2.4. qPCR and gel electrophoresis analyses

qPCR measurements were performed on a CFX96 real-time PCR detection system (Bio-Rad, Hercules, CA, USA) or Eppendorf RealPlex Mastercycler (Hauppauge, NY, USA) with SsoFast™ EvaGreen®

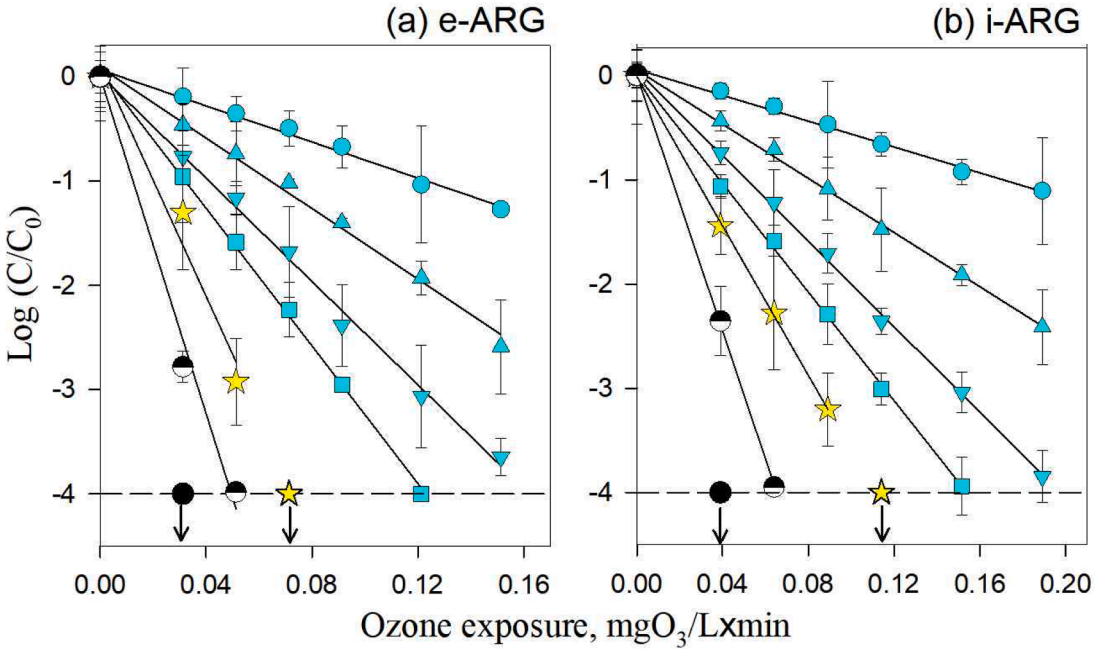

Fig. 1. Logarithmic-scale degradation of *ampR* (192 (●), 400 (▲), 603 (▼) and 851 bps (■)) and elimination of pUC19's transformation activity with *E. coli* DH5α (☆), AB1157 (◓), or AB1886(◒)/AB2463(◐)/AB2480(◑) as recipient strains as a function of O_3 exposure during treatment of (a) extracellular and (b) intracellular pUC19 (*E. coli* DH5α containing pUC19) with O_3 at pH 7 in the presence of *tert*-butanol (10 mM). Symbols represent measured data and error bars represent one standard deviation about the mean from triplicate experiments. Lines are linear regressions of the data, excluding data below the quantification limit (i.e., > 4-log degradation/deactivation, indicated by horizontal dotted lines and symbols with arrows). Note that the symbols for AB1157/AB1886/AB2463/AB2480 appear as (●, solid black) due to the data overlap.

supermixes (Bio-Rad). Four DNA segments with respective lengths of 192, 400, 603, and 851 bp covering varying sections of *amp*^{R} were monitored (Table S1, Figures S1 & S2). pUC19 (1 mg/L) samples before and after FAC and O_3 treatment were analyzed by agarose gel electrophoresis. Further details of the qPCR and gel electrophoresis analyses are provided in SI-Text-3.

2.5. Plasmid transformation assays

Plasmid transformation assays were conducted by using the non-ampicillin resistant *E. coli* K12 wild-type and mutant strains noted above as recipient cells. Further details on the transformation assays are described elsewhere (Nihemaiti et al., 2020; Yoon et al., 2018), and also in SI-Text-4. Concentrations of transformant cells were determined by counting colonies on selective plates containing ampicillin after 24 h of incubation at 37 °C. Final colony counts of recipient cells on nonselective plates without heat shock showed <10% variation (~2 × 10^8 for *E. coli* AB strains and ~3 × 10^8 CFU/mL for *E. coli* DH5α), while final colony counts of transformant cells on selective plates with heat shock showed <50% variation between the *E. coli* strains (Nihemaiti et al., 2020). The transforming activity of pUC19 (efficiency of gene transformation) was calculated as below, and ranged from 10^{-8} to 10^{-4} (Figure S3).

$$\text{Transforming activity} = \frac{Transformant\ cells_{selective\ plate}(CFU/mL)}{Total\ E.coli\ cells_{nonselctive\ plates}(CFU/mL)}$$

2.6. Statistical analyses

Data from independent triplicate experiments were pooled to perform least-squares linear regressions (using GraphPad Prism 7) or nonlinear regressions (using Microsoft Excel Solver) for determining second-order (or pseudo-first-order) rate constants and associated uncertainties (standard errors or deviations) for each *amp*^{R} segment in its reactions with O_3 and FAC. Weighted linear regressions were applied to perform uncertainty-weighted regression analyses of *amp*^{R} segment-specific second-order rate constants vs segment length, or pseudo-first-order rate constants of each segment vs FAC concentrations, according to previously reported methods (He et al., 2019), since these rate constants themselves carry associated uncertainties.

3. Results and discussions

3.1. Degradation of e-ARGs by O_3

Solutions containing pUC19 were exposed to increasing O_3 exposures (0−0.15 $mgO_3/L \times min$) at pH 7 (with $^{\bullet}OH$ scavenged by *tert*-butanol). The results (Fig. 1a) showed that the 192-bp e-*amp*^{R} segment was degraded by ~1.2-log at an O_3 exposure of 0.15 $mgO_3/L \times$ min, whereas a 4-log decrease was achieved for the 851-bps e-*amp*^{R} segment at this O_3 exposure. The degradation of e-*amp*^{R} segments measured by qPCR followed linear kinetics with increasing O_3 exposure ($r^2 = 0.99$, Fig. 1a), indicating first-order reaction kinetics with respect to e-*amp*^{R} and O_3, respectively, and overall second-order reaction kinetics (Choi et al., 2021a). The second-order rate constants for the e-*amp*^{R} segments' degradation by O_3 could be determined from the slopes of the curves shown in Fig. 1a (i.e., $k_{O3,Amp} = 2.303 \times$ slope), and were 1.6(±0.1) × 10^4, 3.1(±0.2) × 10^4, 4.6(±0.3) × 10^4, and 6.1(±0.3) × 10^4 $M^{-1}s^{-1}$ for the 192-, 400-, 603-, and 851-bp segments, respectively (Table 1). The increasing $k_{O3,Amp}$ values of e-*amp*^{R} segments with increasing segment size can be explained by the increasing number of potential O_3 reaction sites on longer segments. Our $k_{O3,Amp}$ values were in good agreement with rate constants previously reported for similar-length segments (266–1017 bp) of the chromosomal *blt* gene of *Bacillus subtilis* (He et al., 2019), indicating similar reactivities of plasmid-borne and chromosomal DNA toward O_3.

The $k_{O3,plasmid}$ of e-pUC19 could be predicted by extrapolating the $k_{O3,Amp}$ of each segment to the entire plasmid (i.e., $k_{O3,plasmid} = k_{O3,Amp} \times \frac{2686bp}{\text{amplicon length}}$, where amplicon length was 192, 400, 603, or 851 bp), based

Table 1
Kinetics parameters for the degradation (qPCR signal loss) and deactivation (loss of transforming activity) of *amp*^{R} during exposure of extracellular (Extra) and intracellular (Intra) plasmid (pUC19) to O_3 and FAC. Mean and standard error values from triplicate experiments are provided, unless otherwise stated in the footnotes.

Oxidant	Plasmid state			Gene degradation (qPCR)					Gene deactivation [c] (transformation assay with *E. coli* strains)		
				amp^R segments				pUC19	DH5α	AB1157	AB1886/ AB2463/ AB2480
			k, $M^{-1}s^{-1}$	192 bps	400 bps	603 bps	851 bps	2686 bps			
O_3	Extra		$k_{O3,Amp}$ pH 7.0	1.6(±0.1)×10^4	3.1(±0.2)×10^4	4.6(±0.3)×10^4	6.1(±0.3)×10^4	2.1(±0.2)×10^5 [a]	1.1(±0.1)×10^5	1.4(±0.1)×10^5	≥2.5×10^5
	Intra		$k_{O3,Amp}$ pH 7.0	1.1(±0.1)×10^4	2.4(±0.2)×10^4	3.8(±0.1)×10^4	4.8±(0.2)×10^4	1.6(±0.2)×10^5 [a]	6.6(±0.5)×10^4	1.1(±0.5)×10^5	≥2.0×10^5
FAC	Extra [b]	With 10 mM *tert*-butanol	$k_{FAC,Amp}$ pH 6.8	2.7(±0.2)×10^3	5.4(±0.5)×10^3	9.2(±0.9)×10^3	1.7(±0.2)×10^4	4.4(±0.7)×10^4	3.6(±0.2)×10^2	-	-
			$k_{FAC,N\text{-}Cl\ bp}$, pH 6.8	2.6(±0.1)×10^{-1}					-		
		without *tert*-butanol	$k_{FAC,Amp}$ pH 6.8	-					5.4(±0.3)×10^2	1.4(±0.2)×10^3	1.5(±0.2)×10^3/ 3.2(±0.1)×10^3/ 4.3(±0.1)×10^3
			$k_{FAC,Amp}$ pH 8.1	-					8.2(±0.2)×10^1	-	-
	Intra		$k_{FAC,Amp}$ pH 6.8	-					1.4(±0.4)×10^2	-	-
			$k_{FAC,Amp}$ pH 8.1	-					1.1(±0.2)×10^2	-	-

[a] k_{pUC19} indicates apparent second-order rate constants for degradation of pUC19 by O_3 which were estimated from the equation obtained from linear regression of the k values for degradation of *amp*^{R} segments (k_{ampR}) by O_3 vs. segment length (Figure S4). The error values of k_{pUC19} were calculated using error propagation for the linear relationship between k_{pUC19} and k_{ampR}.

[b] The degradation of *amp*^{R} segments was modeled by the two-step FAC reaction model as described in the main text (Section 3.4), with $k_{FAC,Amp}$ and $k_{FAC,\ AmpN\text{-}Cl}$ as the rate constants of the first and second steps, respectively, with $k_{FAC,\ AmpN\text{-}Cl}$ values for each *amp*^{R} segment obtained from weighted linear regression of corresponding experimental $k_{obs,\ FAC}$ values over their regions of maximal slope vs. $[FAC]_0$, and with $k_{FAC,N\text{-}Cl\ bp}$ obtained from weighted linear regression of experimental $k_{FAC,AmpN\text{-}Cl}$ values for each *amp*^{R} segment vs. #bp (= #N-Cl bp under conditions of full chlorination). Using the obtained $k_{FAC,N\text{-}Cl\ bp}$ value, the $k_{FAC,Amp}$ values for each segment were determined by fitting of the experimental data with the two-step FAC reaction model. The error values for $k_{FAC,Amp}$ indicate lower and upper values of the model outputs obtained by using the lower and higher range of the standard error of the $k_{FAC,N\text{-}Cl\ bp}$ value, respectively.

[c] Second-order rate constants for the gene (*amp*^{R}) deactivation by O_3 or FAC were determined from the linear slopes of plots of $\log_{10}$-scale transforming activity loss vs oxidant exposure.

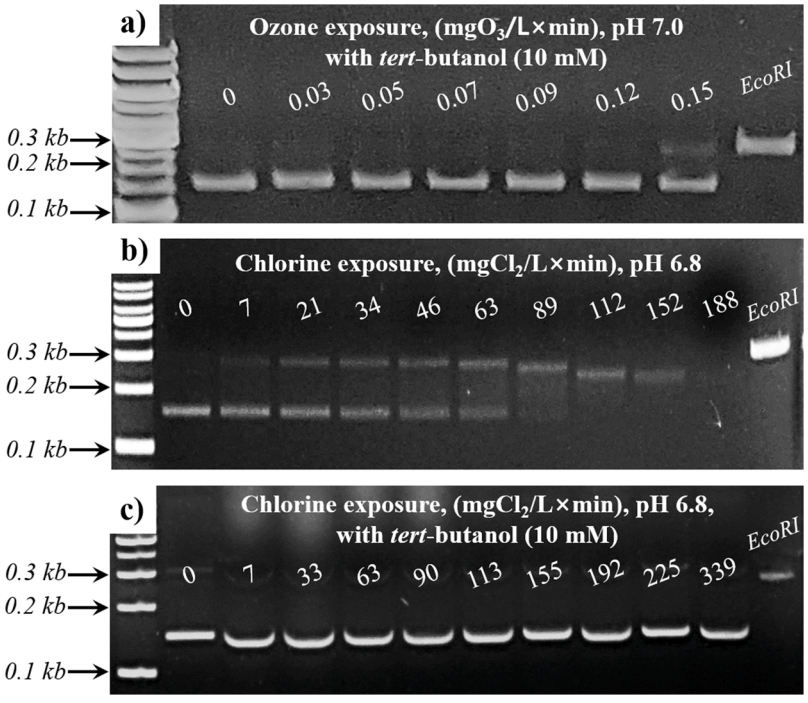

Fig. 2. Agarose gel electrophoresis images of extracellular pUC19 treated with (a) O_3 at pH 7.0 in the presence of *tert*-butanol (10 mM), (b) FAC at pH 6.8 in the absence of *tert*-butanol, and (c) FAC at pH 6.8 in the presence of *tert*-butanol (10 mM). The first column shows gel images of standard ladders. The last column shows gel images of the pUC19 plasmid treated by restriction enzyme (*EcoRI*). The numbers above the gel images indicate the corresponding FAC or O_3 exposures to which the samples were subjected.

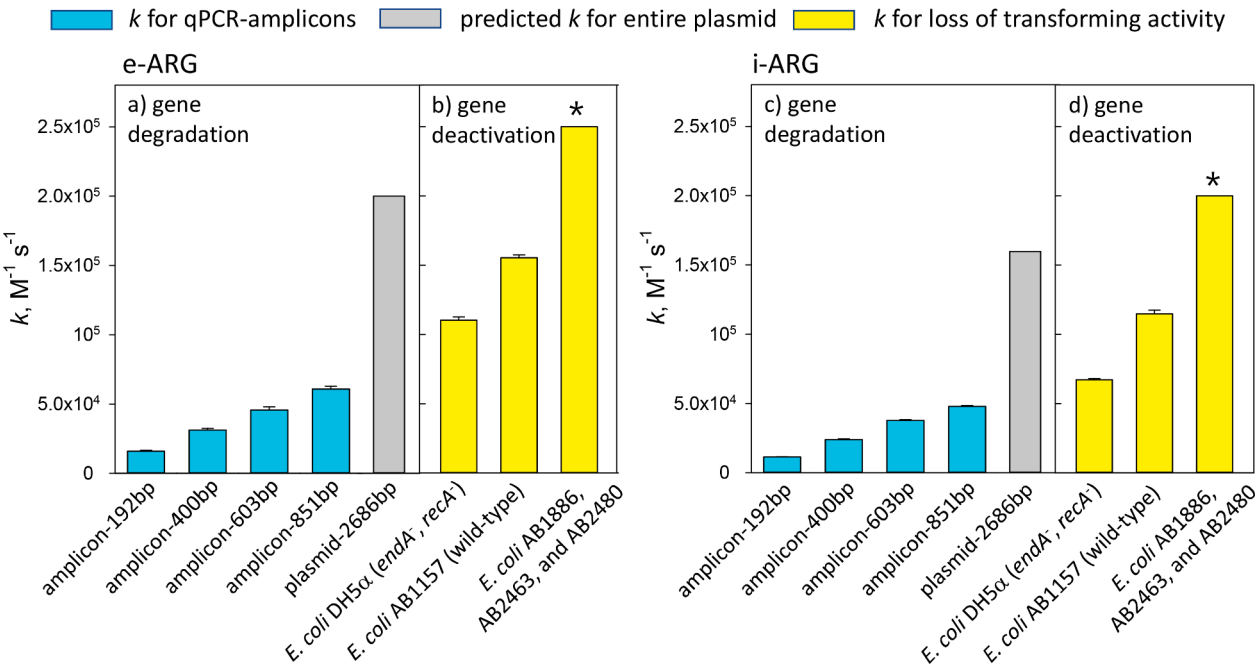

Fig. 3. Apparent second-order rate constants (k) for degradation of amp^R segments (192, 400, 603, and 851 bps) and pUC19 plasmid (2686 bps), and for the loss of pUC19 transforming activity (for *E.coli* strains with varying DNA repair abilities) during O_3 treatments of (a, b) extracellular and (c, d) intracellular ARGs. Error bars of amp^R segment degradation or pUC19 deactivation represent one standard deviation about the mean from triplicate experiments. Error bars of pUC19 degradation represent standard deviations about the means of estimated values from the amp^R segments. The k for pUC19 deactivation using *E. coli* AB1886, AB2463, and AB2480 as recipient strains is the estimated value obtained assuming deactivation to the quantification limit (~4-$\log_{10}$ loss) at the lowest O_3 exposure (designated by * on top of the bars).

on the assumption that the O_3 reactivity per bp is the same across the entire plasmid. The $k_{O3,plasmid}$ values predicted from the 192-, 400-, 603-, and 851-bps segments were 2.2(±0.1) × 10^5, 2.1(±0.1) × 10^5, 2.0 (±0.1) × 10^5, and 1.9(±0.1) × 10^5 $M^{-1}s^{-1}$, respectively, yielding an average $k_{O3,plasmid}$ value of 2.1(±0.2) × 10^5 $M^{-1}s^{-1}$. Alternatively, the $k_{O3,plasmid}$ of the entire plasmid could be predicted by incorporating the total bp number of pUC19 (2686 bps) into the equation resulting from linear regression of $k_{O3,Amp}$ vs. the number of AT+GC bps in each amp^R segment; that is, $k_{O3,Amp}$ (in $M^{-1}s^{-1}$) = 70.7 × (# AT+GC) + (2.4 × 10^3) (Figure S4). This yielded a similar $k_{O3,plasmid}$ value of 1.9(±0.4) × 10^5 $M^{-1}s^{-1}$. The slope of this linear equation (= 71±2 (M AT+GC)$^{-1}s^{-1}$) represents the sequence-independent, average rate constant for the reaction of O_3 with a single base pair of double-stranded (ds) plasmid DNA. A similar value of 65±7 (M AT+GC)$^{-1}s^{-1}$ has been reported for the sequence-independent rate constant for the reaction of O_3 with ds chromosomal DNA, using the *blt* gene (He et al., 2019). Overall, the $k_{O3,plasmid}$ of e-pUC19 is estimated to be ~2 × 10^5 $M^{-1}s^{-1}$ based on the values obtained using the two different methods described above.

Structural change of pUC19 upon exposure to O_3 was investigated by using agarose gel electrophoresis analyses (Fig. 2a). The intact pUC19 before O_3 exposure showed a band at a lower position than the linearized plasmid (i.e., *Eco*RI-treated pUC19), since plasmid DNA normally exists in a supercoiled form, which migrates faster than its linear form in agarose gels. The position of the band for the supercoiled form did not change upon O_3 exposures in the presence of *tert*-butanol (0–0.15 mgO_3/L × min). This suggests that the pUC19 retained its supercoiled structure without significant conformational change such as strand breakage, despite the expected significant level of nucleoside degradation of the plasmid DNA at the applied O_3 exposures. Among nucleosides, the reactivity of O_3 is high with thymidine (3.0 × 10^4 $M^{-1}s^{-1}$) and guanosine (1.6 × 10^4 $M^{-1}s^{-1}$), intermediate with cytidine (3.5 × 10^3 $M^{-1}s^{-1}$), and low with adenosine (16 $M^{-1}s^{-1}$) (Theruvathu et al., 2001) (where the terms in parentheses are k values for the reaction of O_3 with the neutral form of each nucleoside). Consistent with the order of O_3 reactivity of the nucleoside monomers, thymine and guanine bases were found to be the preferential degradation sites in ds plasmid DNA exposed to O_3 (Sawadaishi et al., 1986). Based on a detailed product study with thymine and thymidine (Flyunt et al., 2002), ring opening products caused by C(5)−C(6) double bond cleavage are expected to be formed from the reaction of O_3 with pyrimidine bases. Contrary to the results of the present study, the conversion of plasmid conformation from initial supercoiled to relaxed circular or linear forms was observed in a previous ozonation study (Sawadaishi et al., 1985). This could be due to the formation of $^{\bullet}OH$ from the reaction of O_3 with DNA as it is well known that $^{\bullet}OH$ can induce DNA strand breakage (von Sonntag 2006). In the current study, $^{\bullet}OH$ was fully scavenged by *tert*-butanol, resulting in negligible plasmid conformational change.

3.2. Deactivation of e-ARGs by O_3

The deactivation of e-pUC19 by O_3 was investigated by analyzing the former's transforming activity using non-ampicillin-resistant recipient *E. coli* cells having varying DNA repair abilities. The transforming activity loss rate of O_3-treated e-pUC19 was variable depending on the recipient strain used (Fig. 1a). For the three repair-deficient *E. coli* mutants AB2480 (*uvr*A$^-$, *rec*A$^-$), AB1186 (*uvr*A$^-$), and AB2463 (*rec*A$^-$), no transformant was detectable at the lowest O_3 exposure applied (0.03 mgO_3/L × min), indicating a >4-log decrease (Fig. 1a). By assuming second-order reaction kinetics for e-pUC19 deactivation by O_3, the $k_{O3,transformation}$ value was in turn estimated to be ≥2.5 × 10^5 $M^{-1}s^{-1}$ for the three *E. coli* strains deficient in DNA repair ability. The loss of transforming activity was slower for *E. coli* AB1157 (wild-type) and DH5α (*recA*$^-$, *endA*$^-$) than repair-deficient *E.coli* AB strains, and followed first-order kinetics with respect to O_3. The $k_{O3,transformation}$ values were calculated to be 1.6(±0.3) × 10^5 $M^{-1}s^{-1}$ for AB1157 and 1.0(±0.2) × 10^5 $M^{-1}s^{-1}$ for DH5α from the slopes of plots of $\log_{10}$-scale transforming activity loss vs O_3 exposure (multiplied by a factor of 2.303).

k_{O3} values for the degradation of e-amp^R segments, the full e-pUC19

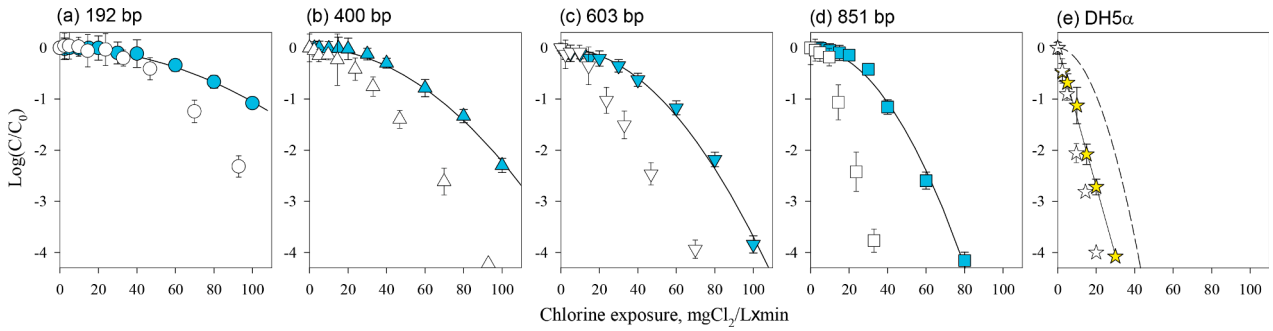

Fig. 4. Logarithmic-scale degradation of (a) 192, (b) 400, (c) 603, and (d) 851 bp *amp*^{R} segments, and (e) elimination of pUC19 transformation activity using *E. coli* DH5α as recipient strain, as a function of FAC exposure during treatment of extracellular pUC19 with FAC at pH 6.8 in the absence (open symbols) and in the presence of *tert*-butanol (10 mM, filled symbols). Symbols represent measured data and error bars represent one standard deviation about the mean from triplicate experiments. Solid lines (black) are non-linear regression lines for *amp*^{R} segments (a–d) or linear regression lines for transforming activity loss (e), each in the presence of *tert*-butanol. The dashed line indicates the model prediction for degradation of pUC19 (e).

plasmid (predicted), and the loss of plasmid transforming activity as measured using the various recipient strains are compared in Fig. 3a and 3b. The estimated degradation rate constant for the entire plasmid (~2 × 10^5 $M^{-1}s^{-1}$, as noted above) overestimated the rate constants for pUC19 deactivation observed for strains AB1157 (wild-type) and DH5α (*recA*$^-$, *endA*$^-$), but the difference in the rate constants was small (differing by factors of 1.3 and 2.1, respectively). The plasmid deactivation rate constant estimated using the three DNA repair-deficient strains was 2.5 × 10^5 $M^{-1}s^{-1}$, which was also close to the predicted degradation rate constant for the entire plasmid (differing by factors of 1.3). These results suggest that every instance of O_3-induced DNA damage (e.g., base oxidation) in pUC19 effectively led to deactivation of the plasmid (loss of transforming activity) when the repair-deficient (*uvr*A$^-$ and/or *rec*A$^-$) *E. coli* strains were used. For the wild-type and DH5α (*recA*$^-$, *endA*$^-$) *E. coli* strains, it appears that not every O_3-induced DNA lesion resulted in plasmid deactivation, due to repair of some fraction of the DNA damage by the recipient cells.

The RecA protein (encoded by the *recA* gene) plays an important role in the repair of single-strand gaps or double-strand breakages by homologous recombination (Shinohara and Ogawa, 1995). The UvrABC proteins (encoded by the *uvr*A, *uvr*B and *uvr*C genes) are responsible for the nucleotide excision repair of various types of DNA lesions, such as the cyclobutane-pyrimidine dimers or 6,4-photoproducts formed during UV irradiation (Kisker et al., 2013). It is possible that RecA or UvrA is also capable of repairing some of the O_3-induced DNA damage, which may explain the lower deactivation rate constant when using the wild-type *E. coli* as a recipient strain compared with the *rec*A and/or *uvr*A deficient strains. Notably, strain DH5α showed the lowest deactivation rate among the tested strains despite its lack of *recA*. The same trend has also been observed during treatment of pUC19 by UV and $^{\bullet}OH$, and explained by the lack of the *endA* gene in DH5α rendering it inherently more active for taking up intact plasmids and thus gene transformation (Nihemaiti et al., 2020).

3.3. Degradation and deactivation of i-ARGs during exposure to O_3

Degradation and deactivation of i-ARGs were investigated by exposing *E. coli* DH5α harboring pUC19 to O_3 at pH 7 in the presence of *tert*-butanol (10 mM). Overall, the kinetic behavior in the degradation and deactivation of i-ARGs (Fig. 1b) was similar to that for e-ARGs (Fig. 1a), and the k_{O3} values of i-ARGs were lower than those of e-ARGs by factors of only 1.2–1.5 ($p < 0.05$) (Table 1). k_{O3} for the degradation of i-*amp*^{R} segments, i-pUC19, and the loss of plasmid transforming activities for the i-ARGs are compared in Fig. 3c and 3d. The $k_{O3,plasmid}$ values predicted from the 192-, 400-, 603-, and 851-bps segments were 1.6 (±0.1) × 10^5, 1.6(±0.1) × 10^5, 1.7(±0.1)× 10^5, and 1.5(±0.1) × 10^5 $M^{-1}s^{-1}$, respectively, yielding an average $k_{O3,plasmid}$ value of 1.6(±0.2) × 10^5 $M^{-1}s^{-1}$. The $k_{O3,transformation}$ values were 1.1(±0.5) × 10^5 $M^{-1}s^{-1}$ for AB1157 and 6.6(±0.5) × 10^4 $M^{-1}s^{-1}$ for DH5α from the slopes of plots of log_{10}-scale transforming activity loss vs O_3 exposure. The predicted i-pUC19 degradation rate constants therefore overestimated the deactivation rate constants by factors of 1.5 and 2.4 for AB1157 and DH5α, respectively. Similar to the case of e-ARGs, the deactivation rate constants for i-ARGs were too fast to be captured by the transformation assays using the three repair-deficient *E. coli* strains (AB1886, AB2463, and AB2480), as shown in Fig. 1b, and a $k_{O3,transformation}$ value for i-ARGs could only be estimated as ≥2 × 10^5 $M^{-1}s^{-1}$ when using these strains (Table 1; Fig. 3d). Overall, our results show that the *E. coli* cell envelope and other cellular constituents did not significantly hinder the ability of O_3 to reach and react with intracellular pUC19.

3.4. Degradation of e-ARGs during exposure to FAC

1) Effect of tert-butanol and involvement of radical reaction. Solutions containing e-pUC19 were exposed to FAC at pH 6.8 at different FAC exposures (0 − 100 $mgCl_2/L$ × min) and quenched with thiosulfate to terminate the reaction. The results (Fig. 4, open symbols) showed that the degradation of e-*amp*^{R} segments became gradually faster with increasing FAC exposure. The degradation rate was lowest for the 192-bp segment, and increased with increasing length of the e-*amp*^{R} segments. It was found that degradation of the e-*amp*^{R} segments in this study was considerably faster than degradation of similar length e-*blt* gene segments in another recent study by our groups (He et al., 2019) when compared at the same FAC exposure. To test whether the faster degradation of the e-*amp*^{R} segment observed in the current study may be related to reactions involving radicals such as $^{\bullet}OH$, e-pUC19 was also exposed to FAC in the presence of *tert*-butanol (10 mM). The results (Fig. 4, filled symbols) showed that degradation of the e-*amp*^{R} segments became significantly slower in the presence of *tert*-butanol.

Agarose gel electrophoresis analyses (Fig. 2b) showed that FAC treatment in the absence of *tert*-butanol resulted in gradual movement of the pUC19 band upward with increasing FAC exposure (0 − 46 $mgCl_2/L$ × min) and then downward with further increase of the FAC exposure (46−188 $mgCl_2/L$ × min). This indicates conformational change of pUC19 from the supercoiled to the linear form and then to another form that migrated faster than the linear form (e.g., fragmented linear plasmid). In contrast, chlorination of pUC19 in the presence of *tert*-butanol (Fig. 2c) did not result in any change in the pUC19 band position at the tested FAC exposures, indicating negligible plasmid conformational variation (e.g., strand breakage) from the initial supercoiled form. The visual trends observed in gel images are also shown in a quantitative manner where the degree of plasmid conformational change is measured as a function of FAC exposure (Figure S5), using quantitative agarose gel image analyses.

The enhanced *amp*^{R} degradation and plasmid conformational changes in the absence of *tert*-butanol indicate an involvement of strong radicals such as $^{\bullet}OH$ during chlorination of the plasmid DNA. Previous studies have also reported formation of single- and double-strand breaks in plasmid DNA during chlorination experiments conducted in the absence of radical scavenger, though such behavior was attributed to formation of N-centered radicals following thermal, metal-, or light-mediated homolysis of N-chlorinated DNA nucleobases (Hawkins and Davies 2002; Suquet et al., 2010). We hypothesize that in the present case, FAC-induced Fenton-like reactions associated with trace metal residues in the DNA extracts may be primarily responsible for radical formation. DNA has high affinity for some transition metals (e.g., Cu(I) and Fe(II)) and the reaction of DNA–metal complexes with FAC (or H_2O_2) is reported to generate $^{\bullet}OH$ (Ouameur et al., 2005; Prütz 1996a, b; Suquet et al., 2010). Even though the plasmids used in this study were purified, they could still have contained trace levels of transition metals in the form of DNA–metal complexes. Separate experiments showed the formation of formaldehyde at concentrations of up to ~70 nM during treatment of pUC19 (2 mg/L) with FAC (70 μM) at pH 7 in the presence of excess *tert*-butanol (50 mM), while formaldehyde formation was negligible during chlorination under the same condition without pUC19 (Figure S6). These data are consistent with formation of $^{\bullet}OH$ in this system, as formaldehyde is one of the major products (with 25% molar yield) from the reaction of $^{\bullet}OH$ with *tert*-butanol (Flyunt et al., 2003a). Further investigation is warranted to test the hypothesis of DNA-metal complexes inducing Fenton-like reactions as a source of radical formation.

It should be noted that *tert*-butanol would likely have little to no effect on reactions driven *directly* by N-centered radicals formed at the DNA nitrogen atoms, as *tert*-butanol is not expected to exhibit significant reactivities toward "weaker" radicals such as $^{\bullet}NH_2$ (Huie, 2003). Accordingly, if N-centered radicals were directly responsible for these reactions, the addition of *tert*-butanol should have little to no effect on the degradation kinetics of e-*amp*^{R} segments and pUC19, in contrast to the observations reported here. However, it may be possible that $Cl^{\bullet}$ formation (and consequently $^{\bullet}OH$ formation via $^{\bullet}Cl + H_2O \leftrightharpoons ClOH^{\bullet-} + H^+ \leftrightharpoons {}^{\bullet}OH + Cl^- + H^+$ or $^{\bullet}Cl + OH^- \leftrightharpoons ClOH^{\bullet-} \leftrightharpoons {}^{\bullet}OH + Cl^-$ (Kläning and Wolff, 1985)) through, for example, thermally- or metal-mediated homolysis of N-chlorinated nucleobases may have contributed *indirectly* to the observed results.

2) Degradation kinetics of amp^R *by FAC.* The observed accelerating kinetics for the degradation of *amp*^{R} segments by direct reactions with FAC (i.e., in the presence of *tert*-butanol) can be interpreted according to a two-step reaction model originally proposed by He et al. He et al., 2019) for chromosomal ARGs (Eqs. (1) and (2)).

$$\mathrm{Amp} + \mathrm{FAC} \underset{\mathrm{Na_2S_2O_3}}{\overset{k_{\mathrm{FAC,Amp}}}{\rightleftharpoons}} \mathrm{Amp_{N\text{-}Cl}} \quad (1)$$

$$\mathrm{Amp_{N\text{-}Cl}} + \mathrm{FAC} \xrightarrow{k_{\mathrm{FAC,Amp\ N\text{-}Cl}}} \mathrm{Product} \quad (2)$$

In this model, an initial reaction between FAC and a hydrogen-bonded nucleotide base pair within a given DNA segment (or amplicon) (Amp) leads to formation of an N-chlorinated DNA segment (or amplicon), $Amp_{N–Cl}$ (the forward step in Eq. (1)), which can be dechlorinated to the parent form upon quenching with a strong reductant such as thiosulfate (the reverse step in Eq. (1)). The heterocyclic NH groups of guanosine and thymidine are the most likely sites of the initial attack represented by Eq. (1), based on their higher reactivities in comparison to the heterocyclic NH or exocyclic NH_2 groups of cytidine or adenosine, or the exocyclic NH_2 group of guanosine (Prütz, 1999; Prütz, 1996a).

In the presence of excess FAC, the fraction of N-chlorinated bases in a given DNA segment ($Amp_{N–Cl}$) will increase with increasing FAC exposure (noting that a segment of DNA can sustain multiple such reversible hits up to a maximum number equal to the number of base pairs in the segment). As the H-bonds between base pairs in the DNA segment are progressively disrupted by N-chlorination, the resulting unpaired nucleobases are activated toward FAC, and may then irreversibly react with FAC to form stable C-chlorinated products that cannot revert to the initial state upon thiosulfate treatment, and that are detectable by qPCR due to blockage of DNA polymerase (Eq. (2)). The observed irreversible degradation kinetics of the DNA segment will gradually increase to a maximum, at which point all nucleotide bases in the segment are N-chlorinated, consistent with the observed linearities of logarithmic-scale *amp*^{R} degradation curves with respect to FAC exposure after reaching a certain threshold range of FAC exposure values (in general > 40–60 $mgCl_2/L \times min$) (Fig. 4, filled symbols). Further details on the two-step FAC reaction model can be found in the prior work (He et al., 2019).

Rate constants for each step of the degradation of *amp*^{R} segments by FAC were determined according to the above model as previously described He et al., 2019). Briefly, $k_{FAC,AmpN–Cl}$ of the second (irreversible) C-chlorination step (Eq. (2)) was firstly determined, and its values were 49.6(±0.7), 93.5(±9.8), 144.2(±4.6), and 219.9(±9.9) $M^{-1}s^{-1}$ for the 192-, 400-, 603-, and 851-bp segments, respectively (Figures S7 and S8). As $k_{FAC,AmpN–Cl}$ can be assumed to be equal to the product of the rate constant for irreversible chlorination of a single N-chlorinated bp ($k_{FAC,N–Cl\ bp}$) and the number of total N-chlorinated bps in a DNA segment (i.e., $k_{FAC,AmpN–Cl} = k_{FAC,N–Cl\ bp} \times$ #N–Cl bp $= k_{FAC,N–Cl\ bp} \times$ #bp, when fully N-chlorinated), an average value of 0.26(±0.01) $M^{-1}s^{-1}$ could be obtained for $k_{FAC,N–Cl\ bp}$ from the slope of a plot of $k_{FAC,AmpN–Cl}$ vs. #bp for each *amp*^{R} segment under conditions of full N–chlorination (Figure S9b). Next, the $k_{FAC,Amp}$ values for the first N-chlorination step (Eq. (1)) were determined for each segment by finding numerical solutions of Eqs. (1) and (2) via non-linear regressions of the experimental data (with $k_{FAC,N–Cl\ bp}$ constant, as determined above, and $k_{FAC,Amp}$ as a master variable to be solved for). Further details of the non-linear regressions are provided in SI-Excel-1. The resulting values of $k_{FAC,Amp}$ were 2.7(±0.2) × 10^3, 5.4(±0.5) × 10^3, 9.2(±0.9) × 10^3, and 1.7(±0.2) × 10^4 $M^{-1}s^{-1}$ for the 192-, 400-, 603-, and 851-bp segments, respectively. Linear regression of these data versus numbers of AT+GC bps per amplicon yielded 16.6±2.7 ($(M\ AT+GC)^{-1}s^{-1}$). The $k_{FAC,Amp}$ values from this study were larger (by a factor of 2 on average) than the reported rate constants for the chromosomally-encoded *blt* and *mecA* genes of *B. subtilis* and *Staphylococcus aureus* (Choi et al., 2021a; He et al., 2019) when compared as the segment length-normalized $k_{FAC,Amp}$ values.

The two-step FAC reaction model could be applied to predict degradation kinetics for the entire e-pUC19 plasmid as a function of FAC exposure, using $k_{FAC,plasmid}$ and $k_{FAC,plasmid\ N–Cl}$ values for degradation of the whole plasmid. $k_{FAC,plasmid}$ was estimated as 5.6(±0.6) × 10^4 $M^{-1}s^{-1}$ by extrapolation from the linear regression equation for $k_{FAC,Amp}$ vs. the number of AT+GC bps in each *amp*^{R} segment, i.e., $k_{FAC,Amp} = (16.6) \times$ (# AT+GC) – (6.0 × 10^3) (Figure S9a). $k_{FAC,plasmid\ N–Cl}$ (for C-chlorination of the fully N-chlorinated plasmid) was estimated as 7.0 × 10^2 $M^{-1}s^{-1}$ from the relationship, $k_{FAC,AmpN–Cl} = k_{FAC,N–Cl\ bps} \times$ #N–Cl bps $= (0.26) \times (2686)$ (Figure S9b). Using these rate constants for the whole plasmid in the two-step FAC reaction model, a degradation profile of pUC19 as a function of FAC exposure was generated, as shown by the dashed line in Fig. 4e. Based on the model prediction, 4-log level degradation of e-pUC19 was achieved at an FAC exposure of ~40 $mgCl_2/L \times min$.

3) Effect of pH. Degradation rate constants for e-*amp*^{R} segments were also examined at pH 8.1 by exposing solutions containing pUC19 to FAC in the absence of *tert*-butanol. The degradation of e-*amp*^{R} segments at pH 8.1 was much slower than at pH 6.8 (both cases in the absence of *tert*-butanol), as shown in Figure S10. The slower degradation of e-*amp*^{R} segments at higher pH could be attributed to the change in FAC speciation from HOCl to less reactive OCl^- ($HOCl \Leftrightarrow H^+ + OCl^-$, $pK_a = 7.5$ (Morris, 1966)). Note that the two-step FAC reaction model was not applied to kinetic data obtained in the absence of *tert*-butanol at pHs 6.8 and 8.1, as these data involve not only FAC, but also likely $^{\bullet}OH$

reactions.

3.5. Deactivation of e-pUC19 during exposure to FAC

The deactivation of e-pUC19 by FAC in the absence of *tert*-butanol at pH 6.8 was compared using the *E. coli* AB and DH5α strains as recipient cells. As observed for O_3, the kinetics of transforming activity loss for FAC-treated e-pUC19 also varied depending on the recipient strain used. In contrast to the accelerating degradation kinetics observed for e-*amp*^{R} segments and e-pUC19, the loss of transforming activity for most *E. coli* strains exhibited linear kinetics with respect to FAC exposure (Fig. 5), and apparent $k_{FAC,transformation}$ values could be obtained from the slopes of the resulting decay curves. The reason for the deviations in kinetic behavior for degradation vs. deactivation is currently unclear.

The rate constants for transforming activity loss decreased in the order of AB2463 (*rec*A$^-$, 3.2×10^3 $M^{-1}s^{-1}$), AB1186 (*uvr*A$^-$, 1.5×10^3 $M^{-1}s^{-1}$), AB1157 (wild-type, 1.4×10^3 $M^{-1}s^{-1}$), and DH5α (*recA*$^-$, *endA*$^-$, 5.4×10^2 $M^{-1}s^{-1}$), where the values in parentheses are $k_{FAC,transformation}$. For the *E. coli* mutant AB2480 (*uvr*A$^-$, *rec*A$^-$), no transformants were detectable even at the lowest FAC exposure applied (2.4 $mgCl_2/L \times min$), indicating *a* >4-log decrease (Fig. 5). By assuming second-order reaction kinetics for e-pUC19 deactivation by FAC (consistent with the trends observed when using the other *E. coli* recipient strains), the $k_{FAC,transformation}$ value was estimated to be $\geq 4 \times 10^3$ $M^{-1}s^{-1}$ when using strain AB2480. Thus, $k_{FAC,transformation}$ for pUC19 deactivation when using the double-mutant AB2480 was ≥4-fold more rapid than when using the wild-type AB1157. $k_{FAC,transformation}$ values for pUC19 deactivation were in general ~2−4-fold higher when using the AB strains as recipients than when using DH5α. Similar trends were observed for O_3, consistent with the various DNA repair abilities of these *E. coli* strains (see the above discussion in the O_3 section).

The deactivation efficiency of e-pUC19 was also determined at pH 8.1, using DH5α as the recipient cell. The result showed that e-pUC19 deactivation kinetics depended strongly on pH, where $k_{FAC,transformation}$ at pH 6.8 (5.4×10^2 $M^{-1}s^{-1}$) was ~7-fold higher than at pH 8.1 (82 $M^{-1}s^{-1}$).

The effect of *tert*-butanol on the kinetics of e-pUC19 deactivation was also investigated. The results showed that deactivation of e-pUC19 (using DH5α as recipient strain) in the absence of *tert*-butanol ($k_{FAC,transformation} = 5.4 \times 10^2$ $M^{-1}s^{-1}$) was faster than in the presence of *tert*-butanol ($k_{FAC,transformation} = 3.6 \times 10^2$ $M^{-1}s^{-1}$) by a factor of 1.5. This behavior is consistent with an additional e-pUC19 degradation pathway induced by radicals during chlorination in the absence of *tert*-butanol. We also attempted to compare deactivation kinetics of pUC19 with degradation kinetics for the entire plasmid (pUC19), each in the presence of *tert*-butanol, in which the two-step FAC reaction model

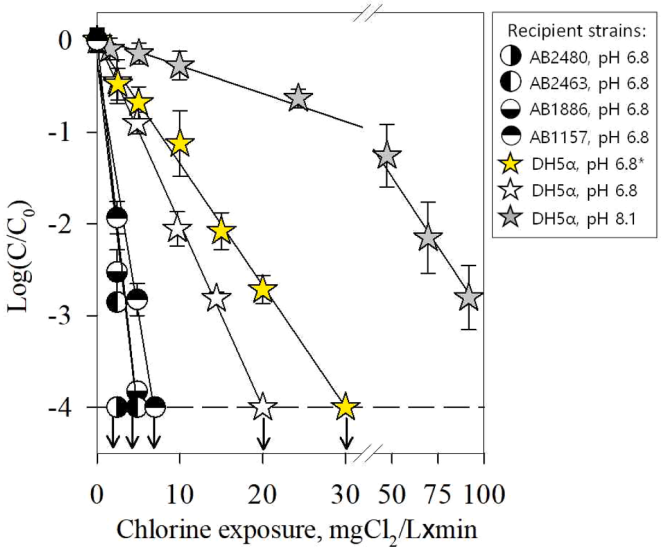

Fig. 5. Logarithmic-scale losses of pUC19 transforming activity as a function of FAC exposure during treatment of extracellular pUC19 with FAC in the absence and presence(*) of *tert*-butanol (10 mM) at pH 6.8 and 8.1. Transforming activities were measured using different *E. coli* strains, including DH5α (☆), AB1157 (◓), AB1886 (◒), AB2463 (◐), and AB2480 (◑). Symbols represent measured data and error bars represent one standard deviation about the mean from triplicate experiments. Lines are linear regressions of the data, excluding data below the quantification limit (i.e., > 4-log deactivation, indicated by the horizontal dotted line and symbols with arrows).

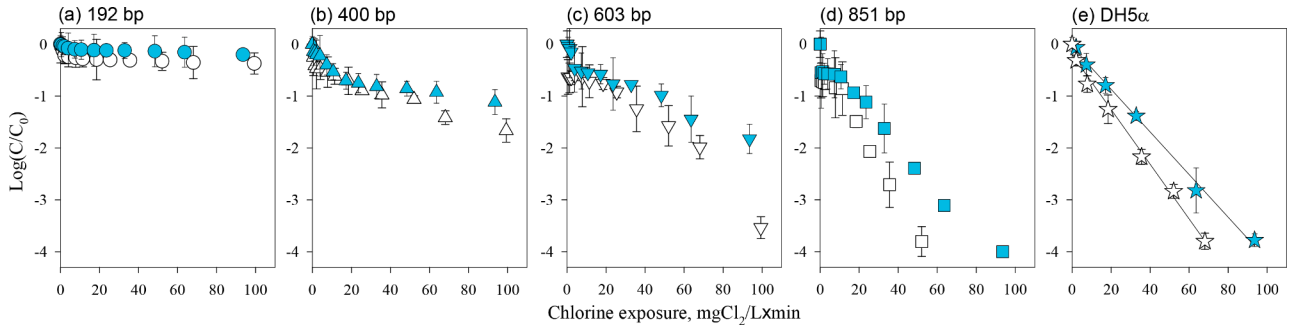

Fig. 6. Logarithmic-scale degradation of (a) 192, (b) 400, (c) 603, and (d) 851 bp i-*amp*^{R} segments, and (e) elimination of pUC19 transforming activity using *E. coli* DH5α recipient strain, as a function of FAC exposure during treatment of intracellular pUC19 (*E. coli* DH5α containing pUC19) with FAC at pH 6.8 (open symbols) and pH 8.1 (filled symbols). Symbols represent measured data and error bars represent one standard deviation about the mean from triplicate experiments. Solid lines are linear regressions of the data for transforming activity losses.

was used to predict the degradation of e-pUC19 as a function of FAC exposure (see Section 3.4). The predicted degradation profile for pUC19 was in reasonable agreement with the experimental deactivation profile for pUC19, aside from the curvature of the predicted degradation profile at low FAC exposures, resulting in overall underestimation of pUC19 deactivation (Fig. 4e). The difference between the degradation model prediction and the experimental deactivation data indicates that there may be other factors unaccounted for by the model that contribute to pUC19 transforming activity loss. Nevertheless, our data show overall that FAC-induced DNA damage in pUC19 effectively leads to deactivation of the plasmid.

3.6. Degradation and deactivation of i-ARGs during exposure to FAC

Degradation of i-ARGs was investigated by exposing cells of *E. coli* DH5α harboring pUC19 to FAC at pH 6.8 and pH 8.1 in the absence of *tert*-butanol. Overall, the kinetic behaviors of i-ARG degradation (Fig. 6) appeared to be different from those of e-ARG degradation (Fig. 4). There was a rapid, initial degradation of i-amp^R segments (0.3 – 0.9 log losses) at FAC exposures of 0.5 – 20 $mgCl_2/L \times min$, whereas this initial rapid loss was not observed for the e-amp^R. After the initial rapid decreases, the degradation of the 603 and 851 bp i-amp^R segments exhibited accelerating kinetics with respect to FAC exposure (more evident under the pH 6.8 conditions), whereas kinetics for the 192 and 400 bp segments were generally closer to linear. Degradation kinetics of i-amp^R segments after the initial rapid losses were similar at pH 6.8 and pH 8.1 (slightly faster at pH 6.8 than pH 8.1), whereas degradation kinetics of e-amp^R segments were significantly higher at pH 6.8 than pH 8.1 (Figure S10). Furthermore, the degradation kinetics of i-amp^R segments at pH 6.8 and pH 8.1 (which were similar) were slower than for e-amp^R at pH 6.8 and faster than for e-amp^R at pH 8.1 (Figures S11 and S12).

The initial rapid loss of i-ARGs was also observed in a previous study (Yoon et al., 2017), and explained by Fenton-like processes initiated within *E. coli* cells by reactions of FAC (following its penetration of the cell envelope) with intracellular metal species (e.g., Fe(II) or Cu(I)) that could generate free radicals and cause oxidative DNA damage. As an alternative hypothesis, decreased efficacy of plasmid DNA recovery from FAC-treated *E. coli* cells (compared with intact cells) might also be responsible for the initial rapid i-ARG loss. However, the degree of initial amp^R loss was found to increase with increasing size of the monitored amp^R segment (Figure S13). This indicates that the initial rapid loss of i-ARGs is more likely related to DNA degradation than to DNA recovery, as in the latter case the degree of observed i-ARG loss would likely be independent of amp^R segment size.

The lack of a substantial pH effect on i-ARG degradation kinetics compared with e-ARGs was also observed in a previous study (Yoon et al., 2017) and explained by the change of FAC speciation after its transport into the cells, due to cytoplasmic pH conditions (pH 7.2 – 7.8) (Wilks and Slonczewski 2007). In this scenario, the reaction of FAC with the i-amp^R would likely have occurred under conditions reflective of e-amp^R degradation at pH ~7.5 (consistent with the fact that i-amp^R degradation kinetics were intermediate between the e-amp^R kinetics observed at pH 6.8 and 8.1).

Deactivation of i-ARGs was also determined for the *E. coli* DH5α exposed to FAC at pH 6.8 and pH 8.1 in the absence of *tert*-butanol. The plasmid was extracted from the chlorinated *E. coli* samples, and applied to the gene transformation assay using non-resistant *E. coli* DH5α. The deactivation kinetics of i-pUC19 at pH 6.8 and pH 8.1 differed by only a factor of ~1.4 (1.4×10^2 $M^{-1}s^{-1}$ and 1.0×10^2 $M^{-1}s^{-1}$, respectively) (Fig. 6e), consistent with the weak pH dependence observed for i-amp^R degradation. FAC exposures of 68 $mgCl_2/L \times min$ at pH 6.8 and 94 $mgCl_2/L \times min$ at pH 8.1 were required to reach 4-log decreases of transforming activity for i-pUC19. The deactivation kinetics of i-pUC19 at pH 6.8 and 8.1 were slower than for e-pUC19 at pH 6.8, but faster than for e-pUC19 at pH 8.1. These trends in i-pUC19 deactivation kinetics are also consistent with a change of FAC speciation in response to the cytoplasmic pH of *E. coli* (~7.5), as discussed above in the context of the observed kinetics of i-amp^R degradation.

4. Conclusions

- Degradation of the amp^R–bearing plasmid pUC19 by O_3 was fast, with a k value of $\sim 2 \times 10^5$ $M^{-1}s^{-1}$. The deactivation of pUC19 by O_3 was also rapid, with k values similar to or slightly lower (within a factor of 2.1) than those for the degradation of pUC19 when assessed using *E. coli* strains with varying DNA repair abilities as recipient cells. Influence of cellular components on the reaction efficiency of O_3 with intracellular plasmids was minor, with e-pUC19 and i-pUC19 degradation and deactivation in generally good agreement.
- Considering the high O_3 reactivity in gene degradation and deactivation, efficient elimination of plasmid-borne ARGs appears to be feasible during ozonation of drinking water and wastewater effluent, though further work with other bacterial strains (including environmental strains), plasmids, and ARGs is needed to confirm these findings can be generalized. Impacts of water matrix components such as suspended solids and dissolved organic matter should also be considered.
- Degradation of pUC19 during chlorination was driven by direct reactions with FAC, as well as by reactions with radicals that may have been generated from incidental reactions of FAC with plasmid DNA extracts.
- The kinetics of direct amp^R segment degradation by FAC accelerated with increasing FAC exposure, and could be described by a two-step sequential reaction model. Degradation of pUC19 by FAC, which could be predicted by the two-step FAC reaction model, lagged the deactivation of the plasmid at low exposures (<10 $mgCl_2/L \times min$), though kinetics of degradation and deactivation were in generally good agreement at higher exposures (>20 $mgCl_2/L \times min$).
- O_3-induced and FAC-induced plasmid DNA damage were repairable by *E. coli* recipient strains, though the extent of DNA repair was lower for the cases of O_3 and FAC when compared to those of UV and $^{\bullet}OH$ determined in previous work (Nihemaiti et al., 2020).
- Overall, significant levels of plasmid-borne ARG degradation and deactivation appear to be achievable during water chlorination, especially for extracellular ARGs at near-neutral pH. As noted above for O_3, further work with other bacterial strains, plasmids, and ARGs, in addition to consideration of water matrix effect (e.g., suspended solids, dissolved organic matter, ammonia), is needed to confirm the degree to which these findings can be generalized.
- The findings from this study and our prior investigations (Nihemaiti et al., 2020; Yoon et al., 2018) support the combination of qPCR analyses and kinetics-based modeling approaches as useful tools to assess and predict the deactivation efficiencies of plasmid-encoded ARGs during water disinfection/oxidation processes.

Declaration of Competing Interest

The authors declare that they have no known competing financial interests or personal relationships that could have appeared to influence the work reported in this paper.

Acknowledgements

This study was supported by the National Research Foundation funded by the Ministry of Science and ICT (NRF-2020R1A2C2011951). Additional support for MCD and HH provided by U.S. National Science Foundation Grant Number CBET-1254929 is gratefully acknowledged.

Supplementary materials

Supplementary material associated with this article can be found, in the online version, at doi:10.1016/j.watres.2021.117408.

References

Alexander, J., Knopp, G., Dötsch, A., Wieland, A., Schwartz, T., 2016. Ozone treatment of conditioned wastewater selects antibiotic resistance genes, opportunistic bacteria, and induce strong population shifts. Sci. Total Environ. 559, 103–112.

Chang, P.H., Juhrend, B., Olson, T.M., Marrs, C.F., Wigginton, K.R., 2017. Degradation of extracellular antibiotic resistance genes with UV254 treatment. Environ. Sci. Technol. 51 (11), 6185–6192.

Choi, Y., He, H., Dodd, M.C., Lee, Y., 2021a. Degradation Kinetics of Antibiotic Resistance Gene mecA of Methicillin-Resistant Staphylococcus aureus (MRSA) during Water Disinfection with Chlorine, Ozone, and Ultraviolet Light. Environ. Sci. Technol. 55 (4), 2541–2552.

Czekalski, N., Berthold, T., Caucci, S., Egli, A., Bürgmann, H., 2012. Increased levels of multiresistant bacteria and resistance genes after wastewater treatment and their dissemination into Lake Geneva, Switzerland. Front. Microbiol. 3, 106.

Czekalski, N., Imminger, S., Salhi, E., Veljkovic, M., Kleffel, K., Drissner, D., Hammes, F., Bürgmann, H., Von Gunten, U., 2016. Inactivation of antibiotic resistant bacteria and resistance genes by ozone: from laboratory experiments to full-scale wastewater treatment. Environ. Sci. Technol. 50 (21), 11862–11871.

Davies, J., Davies, D, 2010. Origins and evolution of antibiotic resistance. Microbiol. Mol. Biol. Rev. 74 (3), 417–433.

Dodd, M.C., 2012. Potential impacts of disinfection processes on elimination and deactivation of antibiotic resistance genes during water and wastewater treatment. J. Environ. Monit. 14 (7), 1754–1771.

Flyunt, R., Leitzke, A., Mark, G., Mvula, E., Reisz, E., Schick, R., von Sonntag, C., 2003a. Determination of •OH, O2•-, and Hydroperoxide Yields in Ozone Reactions in Aqueous Solution. J. Phys. Chem. B 107 (30), 7242–7253.

Flyunt, R., Leitzke, A., Mark, G., Mvula, E., Reisz, E., Schick, R., von Sonntag, C., 2003b. Determination of• OH, O2•-, and hydroperoxide yields in ozone reactions in aqueous solution. J. Phys. Chem. B 107 (30), 7242–7253.

Flyunt, R., Theruvathu, J.A., Leitzke, A., von Sonntag, C., 2002. The reactions of thymine and thymidine with ozone. J. Chem. Soc. 2 (9), 1572–1582. Perkin Transactions.

Hawkins, C.L., Davies, M.J., 2002. Hypochlorite-induced damage to DNA, RNA, and polynucleotides: formation of chloramines and nitrogen-centered radicals. Chem. Res. Toxicol. 15 (1), 83–92.

He, H., Zhou, P., Shimabuku, K.K., Fang, X., Li, S., Lee, Y., Dodd, M.C., 2019. Degradation and deactivation of bacterial antibiotic resistance genes during exposure to free chlorine, monochloramine, chlorine dioxide, ozone, ultraviolet light, and hydroxyl radical. Environ. Sci. Technol. 53 (4), 2013–2026.

Huie, R.E. (2003) NDRL/NIST Solution Kinetics Database on the WEB.

Jacangelo, J.G., Trussell, R.R., 2002. International report: water and wastewater disinfection-trends, issues and practices. Water Sci. Technol.: water supply 2 (3), 147–157.

Kisker, C., Kuper, J., Van Houten, B., 2013. Prokaryotic nucleotide excision repair. Cold Spring Harb. Perspect. Biol. 5 (3), a012591.

Kläning, U.K., Wolff, T., 1985. Laser Flash Photolysis of HClO, ClO−, HBrO, and BrO− in Aqueous Solution. Reactions of Cl-and Br-Atoms. Ber. Bunsenges. Phys. Chem. 89 (3), 243–245.

McKinney, C.W., Pruden, A., 2012. Ultraviolet disinfection of antibiotic resistant bacteria and their antibiotic resistance genes in water and wastewater. Environ. Sci. Technol. 46 (24), 13393–13400.

Morris, J.C., 1966. The acid ionization constant of HOCl from 5 to 35. J. Phys. Chem. 70 (12), 3798–3805.

Nagler, M., Insam, H., Pietramellara, G., Ascher-Jenull, J., 2018. Extracellular DNA in natural environments: features, relevance and applications. Appl. Microbiol. Biotechnol. 102 (15), 6343–6356.

Nihemaiti, M., Yoon, Y., He, H., Dodd, M.C., Croué, J.-.P., Lee, Y., 2020. Degradation and deactivation of a plasmid-encoded extracellular antibiotic resistance gene during separate and combined exposures to UV254 and radicals. Water Res., 115921

Ouameur, A.A., Arakawa, H., Ahmad, R., Naoui, M., Tajmir-Riahi, H., 2005. A comparative study of Fe (II) and Fe (III) interactions with DNA duplex: major and minor grooves bindings. DNA Cell Biol. 24 (6), 394–401.

Pak, G., Salcedo, D.E., Lee, H., Oh, J., Maeng, S.K., Song, K.G., Hong, S.W., Kim, H.-.C., Chandran, K., Kim, S., 2016. Comparison of antibiotic resistance removal efficiencies using ozone disinfection under different pH and suspended solids and humic substance concentrations. Environ. Sci. Technol. 50 (14), 7590–7600.

Prütz, W., 1999. Consecutive halogen transfer between various functional groups induced by reaction of hypohalous acids: NADH oxidation by halogenated amide groups. Arch. Biochem. Biophys. 371 (1), 107–114.

Prütz, W.A., 1996a. Hypochlorous acid interactions with thiols, nucleotides, DNA, and other biological substrates. Arch. Biochem. Biophys. 332 (1), 110–120.

Prütz, W.A., 1996b. Measurement of copper-dependent oxidative DNA damage by HOCl and H2O2 with the ethidium-binding assay. J. Biochem. Biophys. Methods 32 (2), 125–135.

Pruden, A., Pei, R., Storteboom, H., Carlson, K.H., 2006. Antibiotic resistance genes as emerging contaminants: studies in northern Colorado. Environ. Sci. Technol. 40 (23), 7445–7450.

Sawadaishi, K., Miura, K., Ohtsuka, E., Ueda, T., Ishizaki, K., Shinriki, N., 1985. Ozonolysis of supercoiled pBR322 DNA resulting in strand scission to open circular DNA. Nucleic Acids Res. 13 (20), 7183–7194.

Sawadaishi, K., Miura, K., Ohtsuka, E., Ueda, T., Shinriki, N., Ishizaki, K., 1986. Structure-and sequence-specificity of ozone degradation of supercoiled plasmid DNA. Nucleic Acids Res. 14 (3), 1159–1169.

Shinohara, A., Ogawa, T., 1995. Homologous recombination and the roles of double-strand breaks. Trends Biochem. Sci. 20 (10), 387–391.

Suquet, C., Warren, J.J., Seth, N., Hurst, J.K., 2010. Comparative study of HOCl-inflicted damage to bacterial DNA ex vivo and within cells. Arch. Biochem. Biophys. 493 (2), 135–142.

Theruvathu, J.A., Flyunt, R., Aravindakumar, C.T., von Sonntag, C., 2001. Rate constants of ozone reactions with DNA, its constituents and related compounds. J. Chem. Soc., Perkin Trans. 2 (3), 269–274.

Thomas, C.M., Nielsen, K.M., 2005. Mechanisms of, and barriers to, horizontal gene transfer between bacteria. Nat. Rev. Microbiol. 3 (9), 711.

United Nations, 2019. No Time to Wait: Securing the Future from Drug-Resistant Infections. Report to the Secretary-General of the United Nations.

von Gunten, U., 2018. Oxidation processes in water treatment: are we on track? Environ. Sci. Technol. 52 (9), 5062–5075.

von Sonntag, C., 2006. Free-radical-induced DNA Damage and Its Repair. Springer.

Von Sonntag, C., Von Gunten, U., 2012. Chemistry of Ozone in Water and Wastewater Treatment. IWA publishing.

Wilks, J.C., Slonczewski, J.L., 2007. pH of the cytoplasm and periplasm of Escherichia coli: rapid measurement by green fluorescent protein fluorimetry. J. Bacteriol. 189 (15), 5601–5607.

Yoon, Y., Chung, H.J., Di, D.Y.W., Dodd, M.C., Hur, H.-.G., Lee, Y., 2017. Inactivation efficiency of plasmid-encoded antibiotic resistance genes during water treatment with chlorine, UV, and UV/H2O2. Water Res. 123, 783–793.

Yoon, Y., Dodd, M.C., Lee, Y., 2018. Elimination of transforming activity and gene degradation during UV and UV/H 2 O 2 treatment of plasmid-encoded antibiotic resistance genes. Environ. Sci.: Water Res. Technol. 4 (9), 1239–1251.

Zhang, M., Chen, S., Yu, X., Vikesland, P., Pruden, A., 2019. Degradation of extracellular genomic, plasmid DNA and specific antibiotic resistance genes by chlorination. Front. Environ. Sci. Eng. 13 (3), 1–12.

Zhang, Y., Li, A., Dai, T., Li, F., Xie, H., Chen, L., Wen, D, 2018. Cell-free DNA: a neglected source for antibiotic resistance genes spreading from WWTPs. Environ. Sci. Technol. 52 (1), 248–257.